Clean Technologies and Environmental Policy (2020) 22:773–786
https://doi.org/10.1007/s10098-019-01792-z

ORIGINAL PAPER

Feasibility assessment of removal of heavy metals and soluble microbial products from aqueous solutions using eggshell wastes

Revathy Sankaran[1] · Pau Loke Show[2] · Chien-Wei Ooi[3] · Tau Chuan Ling[1] · Chen Shu-Jen[4] · Siao-Ying Chen[5] · Yu-Kaung Chang[5]

Received: 30 October 2019 / Accepted: 9 December 2019 / Published online: 3 January 2020

Abstract

The effective removal of heavy metals and soluble microbial products from wastewater is crucial for ensuring a safe environment and good quality human health. The present work investigated the potential of eggshell (ES) waste as an adsorbent for removing heavy metals and soluble microbial products. ES was firstly used to capture heavy metal ions, and the eggshell–metal (ES-M) complex was then applied to remove soluble microbial products (e.g., proteins) from aqueous solution. In this study, bovine serum albumin (BSA) was selected as a model protein-based contaminant. The equilibrium and kinetic characteristics of soluble protein removed by ES were evaluated in batch mode involving parameters such as metal ions (Cu^{2+}, Zn^{2+}, Ni^{2+}, Co^{2+}), operating temperatures (277–323 K), and particle size of ES (100–700 µm). The isotherm curves were well-fitted by Langmuir–Freundlich model. As the temperature increased from 277 to 323 K, the maximum binding capacity for BSA increased from 25.22 to 34.28 (mg BSA/g ES-Zn). The negative values of ΔG° indicated the spontaneous nature of the protein adsorption, while the kinetic of protein adsorption followed the pseudo-second-order model. ES functionalized with heavy metal ions acted as an effective pseudo-chelating adsorbent for the removal of soluble protein from wastewater. Chelates of Zn–BSA found on the ES complexes were found to be highly stable, indicating a minimal possibility of secondary pollution caused by these Zn- and BSA-containing ES complexes. The ES-Zn complex can be potentially used as an adsorbent for removing soluble microbial products in wastewater prior to the membrane filtration.

Graphic abstract

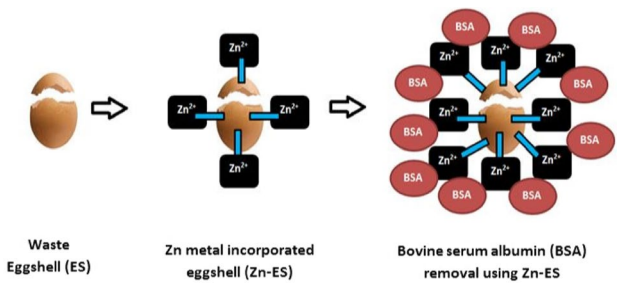

Keywords Eggshell · Adsorbent · Heavy metal · Soluble microbial product · Thermodynamic · Kinetic

✉ Yu-Kaung Chang
ykchang@mail.mcut.edu.tw

Extended author information available on the last page of the article

Highlights

- Potential application of eggshell waste as an adsorbent for removing heavy metals and soluble microbial products.
- Bovine serum albumin selected as a model protein-based contaminant.
- Isotherm curves well-fitted with Langmuir–Freundlich (L–F) model.
- High maximum BSA adsorption capacity with 33.47 mg/g was attained.

Introduction

Lately, water pollution caused by heavy metals has been an increasing environmental and worldwide public health concern associated with environmental contamination. Environmental contamination arises via leaching of heavy metals, metal corrosion, and soil erosion of metal ions, which contaminate groundwater and drinking water. Drinking water which is contaminated with heavy metals is hazardous to human health as they become toxic when they are not metabolized by the body and accumulate in the soft tissues. Various water treatment techniques have been used to remove pollutants from the contaminated water. Among the methods used, adsorption is one of the most commonly used methods and is currently considered to be an efficient and economical process in water purification processes (Jiuhui 2008). There are various adsorbents that can be used for the removal of pollutant, such as activated carbon (Dizge and Tansel 2011), clay minerals (Abollino et al. 2003), zeolites (Oliveira et al. 2004), metal oxides (Zhang et al. 2008), agricultural wastes (Robinson et al. 2002), biomass (Loukidou et al. 2003), and polymeric materials (Atia et al. 2003).

Among these adsorbents, activated carbon has been the most popular and widely used adsorbent in water purification all over the world (Babel and Kurniawan 2003). Activated carbon has a great capacity for adsorbing various organic compounds, and it can be easily modified by chemical treatment to increase the adsorption capacity. However, activated carbon is expensive, and the powdered activated carbon is difficult to be separated from the aquatic system when it becomes exhausted or the effluent reaches the maximum allowable discharge level. For practical use, bio-adsorbent derived from low-cost material or solid waste (Tran et al. 2015) can be efficiently and economically used in the removal of wastes (e.g., heavy metals and soluble proteins) from wastewater (Barker and Stuckey 1999). Eggshell (ES) is the most significant by-product generated from the food industry. Around eight million tons of the ES waste is produced per year worldwide, causing a serious global environmental issue (De Angelis et al. 2017).

ES has been successfully used in removing numerous pollutants including heavy metals and dyes, with the removal efficiency reported in the range of 94–98% (Al-Ghouti and Salih 2018). The porous structure (7000–17,000 pores) of ES makes it an attractive natural bio-adsorbent for the removal of heavy metal ions from wastewater (Stadelman 2000; Wu 2014). Moreover, ES absorbed with heavy metal ion (e.g., Cu^{2+}, Zn^{2+}, Ni^{2+}, Co^{2+}) can be transformed into a pseudo-metal ion-chelating (MIC) adsorbent. The heavy metal ion captured by ES could be derived from industrial wastewater containing heavy metal, thereby preventing secondary pollution during the preparation of MIC adsorbent. The transition metal ions can act as the binding sites for some residues of amino acid in proteins: for example, imidazole group of histidine, thiol group of cysteine (Trzaskowski et al. 2007), indolyl group of tryptophan (Dunbar et al. 2009), and dicarboxylic groups of aspartate and glutamate (Ahmed et al. 1998). Hence, the heavy metal ion decorated onto the ES can improve the binding affinity of ES for the proteins derived from various sources including wastewater (Jarusutthirak and Amy 2006).

SMP is a group of organic compounds derived from substrate metabolism and biomass decay (Kunacheva and Stuckey 2014). SMP consists of polysaccharides, proteins, nucleic acids, organic acids, amino acids, antibiotics, steroids, extracellular enzymes, structural components of cells, and products of energy metabolism. The soluble proteins are the major component in wastewater and are known to cause biological contamination in membrane filtration. SMP was deemed as the component responsible for the membrane fouling and flux decline in wastewater treatment (Jarusutthirak and Amy 2006). The presence of SMP in effluent leads to several undesirable consequences, including (1) changes in color and odor of effluent, (2) higher doses of coagulant and disinfectant required for subsequent treatment, (3) promotion of biological growth, (4) increment in heavy metal and organic pollutant contents (Matilainen et al. 2010), and (5) higher risk of toxicity by-products formation during the chlorination process (Smith et al. 2014). Hence, there exists a need for an effective pretreatment step for membrane filtration used in wastewater treatment.

There are several approaches to convert ES waste into new material for various industrial applications. In this study, MIC adsorbent was prepared by capturing the metallic ion (e.g., M: Cu^{2+}, Zn^{2+}, Ni^{2+}, Co^{2+}) onto the ES waste (namely ES-M). Bovine serum albumin (BSA) was used as a model soluble protein due to its extensive application in biological studies and its interaction with the heavy metals (Masuoka et al. 1993).

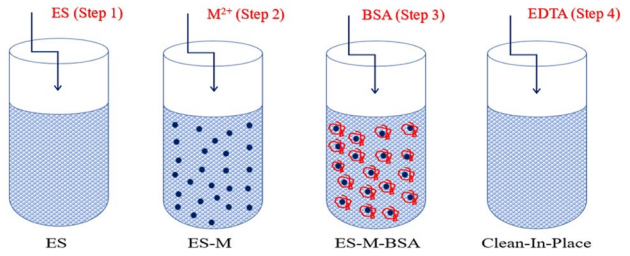

Fig. 1 Operating procedures of removal of heavy metals and soluble microbial products using ES waste

In this work, the feasibility of ES-M complex as a MIC adsorbent for the effective removal of soluble protein (BSA) was examined. The proposed strategy for removing heavy metal ions and soluble proteins with ES waste is shown in Fig. 1. The equilibrium and kinetic characteristics of protein adsorption were investigated, and the efficiency of BSA adsorption by the synthesized ES-M complexes was analyzed. This work could contribute to innovative and cost-effective technology for treating the heavy metal ion and biological wastewaters.

Experimental

Materials

Chicken ES was collected from a local restaurant in New Taipei City, Taiwan. The ES was immersed in 10% NaOH until the impurities and shell membranes were removed. The ES was then washed with deionized water and was completely dried at 105 °C. The dried ES was crushed and sieved into different sizes (i.e., 100–200, 200–300, 300–500, and 500–700 μm). BSA and other chemicals were purchased from Sigma-Aldrich (USA).

Physical characterization

The properties of ES (surface area, pore diameter, and pore volume) were evaluated using N_2 adsorption–desorption isotherms generated by ASAP 2010 apparatus (Micromeritics Co., USA) at − 196 °C. Brunauer–Emmett–Teller (BET) surface area (SBET, m^2/g) and total pore volume (V_t, cm^3/g at STP) were calculated using the N_2 adsorption data. The differential pore-volume distribution pattern was determined according to Barrett–Joyner–Halenda (BJH) method. BJH technique characterizes pore size distribution independent of external area due to the particle size of the sample. The textures of the ES and ES-Zn complex were examined using a scanning electron microscope (model JXA-840, JEOL) with 20 kV of accelerating voltage.

Chemical characterization

X-ray diffraction (XRD) was accomplished by using a diffractometer (model D8, Bruker; 40 kV and 40 mA) with Cu Kα radiation ($\lambda = 0.154$ nm). The patterns of the ES particles and ES-Zn complexes at different ranges of size (100–200, 200–300, 300–500, and 500–700 μm) were examined in the range of 20–80° with a scan speed of 0.03°/s.

Determination of BSA concentration

The concentration of BSA was determined using Bradford method. In brief, an aliquot of sample (20 μL) was incubated with 1 mL of assay reagent for 10 min at a temperature of 25 °C. The absorbance of the mixture was then measured at 595 nm using an ultraviolet–visible (UV–Vis) spectrophotometer (model Ultrospec 3100 pro, GE Healthcare).

Preparation of ES-M adsorbents

Metal ion (e.g., Cu^{2+}, Zn^{2+}, Ni^{2+}, and Co^{2+}) was used for this study. Five grams of ES particle was incubated with 25 mL of metal ion solution (0.1 M sulfate salts in distilled water) in 50 mL centrifuge tubes. The tube was then mixed by a rotary mixer at 20 rpm and 25 °C for 24 h. Supernatant was collected for quantification of metal ion concentration by atomic absorption spectrophotometer.

Selection of solution pH for adsorption of BSA

The removal of BSA from aqueous solution using Zn-decorated ES (ES-Zn) adsorbents was investigated in various buffer solutions (20 mM sodium acetate, pH 4–5; 20 mM sodium phosphate, pH 6–8; 20 mM glycine–NaOH, pH 9–10; 20 mM sodium carbonate, pH 11–12). 0.2 g of ES-Zn adsorbent and 2 mg/mL BSA (5 mL, pH 4–12) were mixed in a 15-mL centrifuge tube using a rotary mixer (Labinco Digital) at 20 rpm and 25 °C for 24 h. The volume of BSA adsorbed on ES-Zn adsorbents (mg BSA/g ES-Zn) was determined by analyzing the mass balance in both liquid and solid phases.

BSA adsorption in batch mode

For batch isotherm and kinetic studies, the experiments were conducted in 15-mL centrifuge tubes containing 0.2 g of ES-Zn adsorbent and 5 mL of BSA (2 mg/mL) in 20 mM sodium acetate buffer at pH 5. All the tubes were sealed and mixed in a rotary mixer at a constant rate of 20 rpm.

BSA sample was removed from the tube after a specified duration of incubation. The solution was centrifuged, and the supernatant was collected for analysis of concentration of residue BSA. The amount of adsorbed BSA was calculated from the mass balance equation. A total of 12 h was used as the contact time for the equilibrium study. The initial BSA concentration (0.2–2.0 mg/mL), temperature (277–323 K), contact time (0–12 h), and ES-Zn sizes (i.e., 100–200 μm, 200–300 μm, 300–500 μm, and 500–700 μm) were examined.

Regeneration and repeated use of ES particle

The multi-step regeneration scheme was used to investigate the capacity of ES (100–1000 mM imidazole or EDTA, 10 mL and 30 min in each step) for BSA adsorption. The solution was centrifuged, and the supernatant was collected for analysis of concentration of residue BSA. The amount of eluted BSA was calculated from the equation of mass balance. The repeated batch of BSA adsorption using ES-Zn adsorbents was performed at 25 °C and 20 rpm for 1 h.

Calculation

For the BSA adsorption study, the amount of BSA removed by the ES-Zn adsorbents was calculated using Eq. 1:

$$q = \frac{V(C_o - C_f)}{w} \tag{1}$$

where C_o and C_f (mg BSA/mL solution) are the initial and the final concentrations of BSA in aqueous phase, respectively; q (mg BSA/g ES-Zn) is the binding capacity of ES-Zn adsorbents. V is the volume of aqueous phase (mL); w is the weight of ES-Zn adsorbents (g).

Isotherm and kinetic models

For the equilibrium isotherm studies, the adsorption data were fitted into the following equilibrium isotherm models, namely Langmuir, Freundlich, and Langmuir–Freundlich models.

The thermodynamic adsorption of BSA by using ES-Zn adsorbents was evaluated by calculating the change in parameters in free energy ($\Delta G°$), enthalpy ($\Delta H°$), and entropy ($\Delta S°$). These parameters can be calculated using the following equations:

$$\Delta G^{\circ} = -RT \ln K_{eq} \tag{2}$$

$$\ln K_{eq} = \left(\frac{\Delta S^{\circ}}{R}\right) - \left(\frac{\Delta H^{\circ}}{R}\right)\frac{1}{T} \tag{3}$$

where R is the universal gas constant (8.314 J/mol K); T is the temperature (K); and K_{eq} (i.e., K_L) is the equilibrium association constant (mL solution/mg BSA). $\Delta H°$ and $\Delta S°$ parameters were obtained from the slope and intercept of the van't Hoff plot of $\ln K_{eq}$ versus $1/T$, respectively.

Kinetic studies

For the BSA adsorption kinetics, the investigation on the controlling mechanism of BSA adsorption was done by using three different kinetic models to fit the experimental data and to derive the rate constants for BSA adsorption:

$$\ln\left(q_{eq} - q_t\right) = \ln q_{eq} - k_1 t \tag{4}$$

$$\left(\frac{t}{q_t}\right) = \left(\frac{1}{k_2 q_{eq}^2}\right) - \left(\frac{1}{q_{eq}}\right)t \tag{5}$$

$$q_t = k_i t^{0.5} + A \tag{6}$$

where q_{eq} and q_t are the concentrations of adsorbed BSA at equilibrium and at contact time t (mg/g), respectively; k_1 and k_2 are the rate constants of the first-order and second-order kinetics, respectively; A is the intercept; k_i is the intra-particle diffusion rate constant (mg/g $\text{min}^{0.5}$).

Results and discussion

Characteristics of ES particles

Table 1 shows the BET surface area, pore diameter, and pore volume of ES particles in different size ranges. Based on the result, it can be deduced that the small size of ES contributes to the larger surface area and pore volume. ES particles mainly consist of fibrous proteins or collagen-like

Table 1 Pore properties of ES particles

Particles size (μm)	BET surface area (m^2/g)	Pore diameter (Å)	Pore volume (cm^3/g)
100–200	0.693	195	0.00337
200–300	0.511	200	0.00319
300–500	0.273	239	0.00176
500–700	0.256	258	0.00153

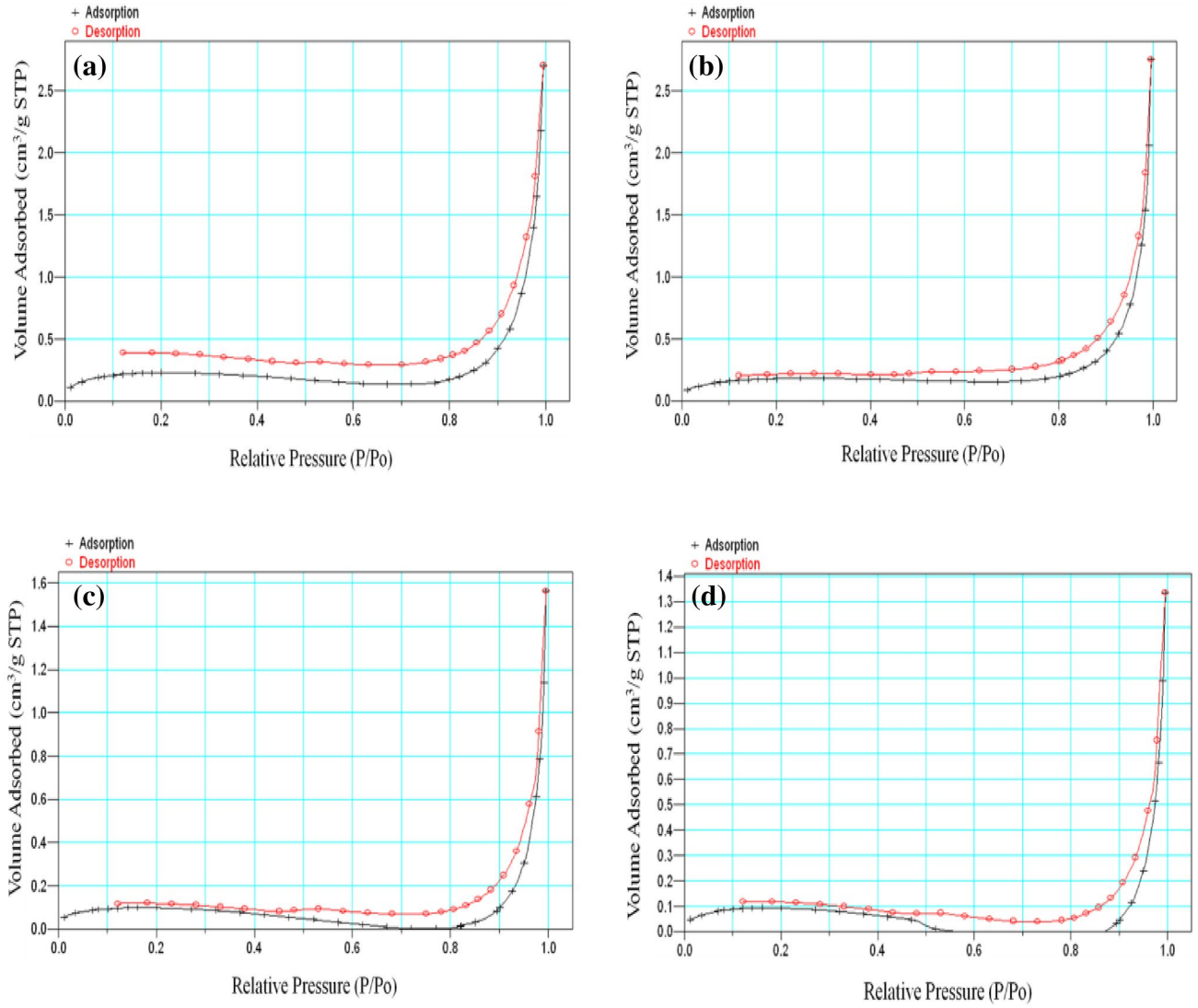

Fig. 2 N_2 adsorption–desorption isotherms of ES particles with particle size in the ranges of **a** 100–200 µm, **b** 200–300 µm, **c** 300–500 µm, and **d** 500–700 µm

proteins. This gives rise to the macropore structure in ES due to the intrinsic existence of the pore canal (Tsai et al. 2006). ES particles in the size range of 100–200 µm had the largest surface (0.693 m^2/g) and the largest pore diameter (0.00337 cm^3/g). From the N_2 isotherm shown in Fig. 2, ES particle with a small size range (i.e., 100–200 µm) was desirable for adsorption of BSA due to its high volumetric area as compared to that of the ES with a larger range of particle size (500–700 µm). This result was in accordance with the results of BET surface area, showing that the small-size ES particle has a bigger surface area available for adsorption. The surface analysis based on BET and BJH models indicated that the specific surface areas of ES were between 0.256 m^2/g (500–700 µm of ES particle) and 0.693 m^2/g (100–200 µm of ES particle). The specific surface area decreased with an increase in ES size. In contrast, the size of the pores increased with an increase in ES size. The sizes of the pores were between 19.5 nm (100–200 µm of ES particle) and 25.8 nm (500–2700 µm of ES particle). Similarly, BJH analysis revealed the non-uniformity of pore size and pore structure in ES-Zn particle.

The textures of ES and ES-Zn complex were analyzed with SEM, and the images are shown in Fig. 3. Based on the SEM images, the structure of raw ES was in an angular pattern, whereas the ES-Zn complex had a crystalline structure with platelets laid on the surface. These observations corroborated the results of surface analysis reported by others (Tsai et al. 2006), in which the outer and inner layers of raw ES are porous in structure. This porous structure makes ES an attractive bio-adsorbent due to the high adsorption capacity. The

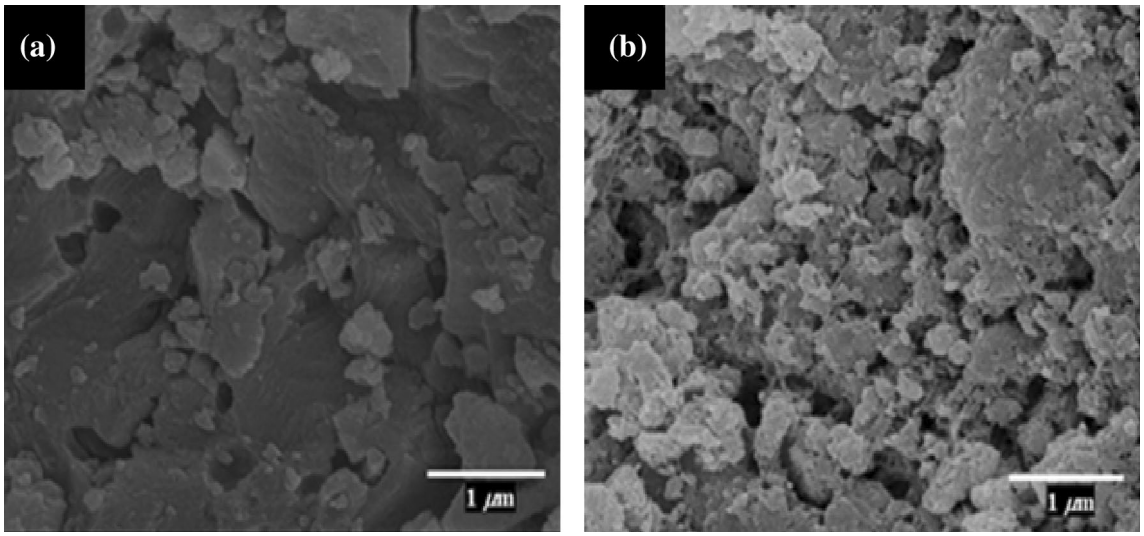

Fig. 3 SEM images of **a** raw ES and **b** ES-Zn complex

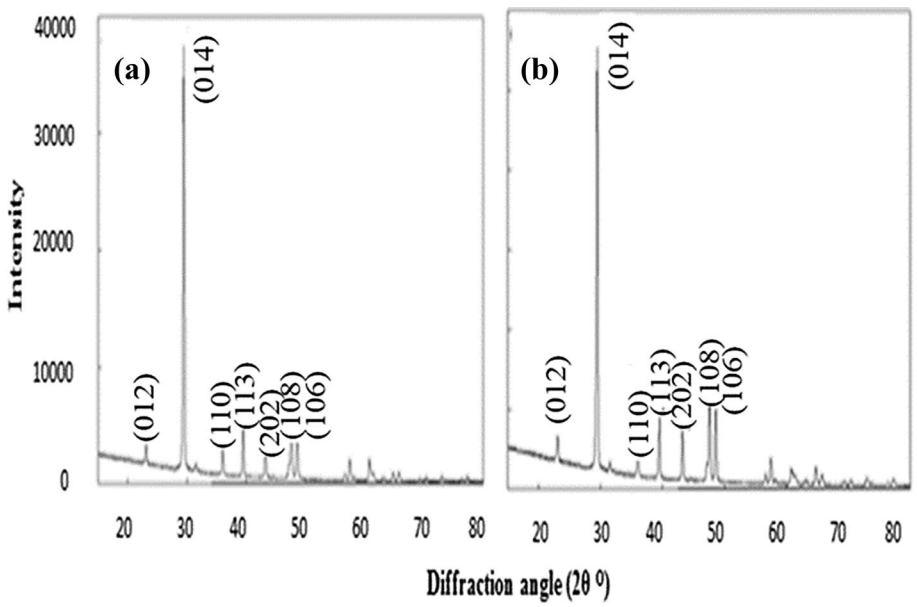

Fig. 4 XRD patterns of **a** raw ES and **b** ES-Zn complex

external surface of ES majorly comprises calcium carbonate, while the inner layer comprises the un-calcified fibrous membranes that are mostly organic compounds (Podstawczyk et al. 2014). Based on Fig. 3, it was revealed that the immobilization of Zn onto the ES increased the porosity of the ES-Zn complex as compared to that of raw ES. This was possibly due to the release of CO_2 within the structure as a result of calcination (Mosaddegh and Hassankhani 2014). The presence of several functional groups (e.g., β-galactosidase, amines and amides) in the ES may possibly assist in the Zn immobilization, which subsequently increases the porosity of ES-Zn complex (Pachapur et al. 2017).

XRD patterns of ES and ES-Zn complex are shown in Fig. 4. The XRD pattern of ES particles matches closely with those stated in the literature (Mosaddegh and Hassankhani 2014). The XRD pattern of ES was also similar to the commercially available $CaCO_3$, wherein the peaks found at $2\theta = 29.4°$ signify that calcite ($CaCO_3$) is the main component of ES. The diffraction pattern of peak of the ES-Zn complex is similar to that of ES but with a lower peak intensity. The low intensity of peak was possibly due to the transformation of the $CaCO_3$ to CaO phase.

Selection of metal ion attached onto ES

The types of metals and metal oxides attached to ES can strongly affect the structural, textural and other characteristics of the resulted ES-M complex (Mopoung and Jitchaijaroenkul 2017). In this case, Zn shows a stronger binding effect. The possible mechanisms involved in the uptake of metal ion by ES are as follows: (1) the cationic exchange properties of metal and the calcium ion exchange process and/or (2) electrostatic interaction between the negative charge species (e.g., carbonate ion) and the positive charge metal ions (Shaheen et al. 2013). The strong affinity between ES and metal ion makes ES-M a perfect candidate for MIC adsorbent for BSA removal. The adsorption behavior of BSA onto the ES-M complex was further investigated.

It is known that the $CaCO_3$ constitutes more than 90% of ES's chemical composition (Zaman et al. 2018). The dissolution of ES can be estimated by the percentage of $CaCO_3$ dissolved in the solution: in the range of pH 4–10, the percentage of $CaCO_3$ dissolved was in the range of 0.24–0.99% (w/w) (Jeppu and Clement 2012). In the presence of water, $CaCO_3$ would undergo displacement reaction according to Eq. 7. ES will possibly dissolve partially and release Ca^{2+}, CO_3^{2-}, HCO_3^-, and OH^- ions (Pramanpol and Nitayapat 2006):

$$CaCO_3 + H_2O \Leftrightarrow Ca^{2+} + HCO_3^- + OH^- + CO_3^{2-} \quad (7)$$

These ions may be adsorbed onto the surface of the ESs, rendering the negative charge properties of ES (Zulfikar et al. 2012). Simultaneously, Ca^{2+} originated from the ES can be exchanged by other metal ions from the surrounding. Hence, the positively charged metal ions would be adsorbed on the negatively charged surface of ES. In this work, it is expected that the Zn ions were adsorbed by the ES via electrostatic interaction and/or cation exchange process.

Choice of pH for BSA adsorption

An alteration in pH may result in the changes in the ionic configuration of the active binding site of the protein and the modification of the conformational shape of the protein molecules (Di Russo et al. 2012). Hence, pH plays a vital role in controlling the adsorption of the compound on the porous materials. The molecular weight and isoelectric point (*p*I) of BSA are 66,411 g/mol and 4.8, respectively (Shi et al. 2008). In BSA molecules, the net negative charge density is mostly centered in N-terminal domain and was the least in the C-terminal domain. Additionally, isomers of BSA exist at various pH conditions (Shi et al. 2008). These properties could affect the interactive behavior between ES-M complex (M: Cu, Zn, Ni, and Co) and BSA molecules. As shown in Fig. 5a, higher pH value in the range of 9–12 did not promote the adsorption of BSA on ES-M adsorbent. This was due to the carbonate and hydroxide ions being the predominant species in a high pH condition, causing the formation of insoluble metal complexes. Hence, the metal complexes cause a decrease in the density of decorated metal ions on the surface of ES-M complex. Moreover, a decrease in the release of Ca^{2+} from ES-M adsorbent would weaken the exchange capacity of M^{2+}, causing a reduction in the binding capacity of ES-M adsorbent for BSA molecules.

The binding capacity of ES-M adsorbent for BSA was weaker when the pH of the solution was lower than the *p*I of BSA. This is due to the repulsive force between the positively charged metal ions and BSA molecules. As shown in Fig. 5a, the maximum binding capacities of different ES-M adsorbents at their optimal pH values were 32.57 mg/g (ES-Zn; pH 5), 30.12 mg/g (ES-Cu; pH 6), 2.56 mg/g (ES-Co; pH 7), 0.28 mg/g (ES-Ni; pH 8). Among these ES-M adsorbents, the most effective

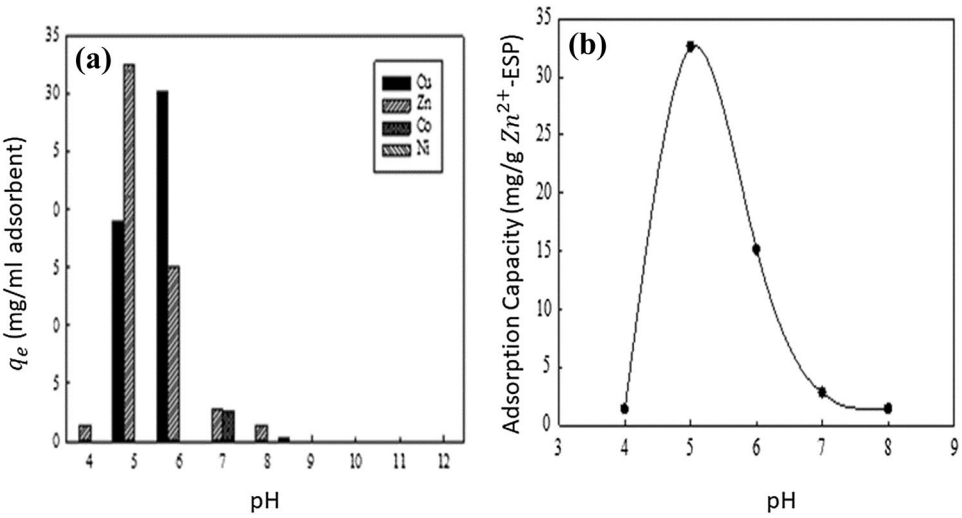

Fig. 5 Effect of pH on BSA adsorption at 298 K by **a** ES-M and **b** ES-Zn complexes

removal of BSA was attained by ES-Zn adsorbent at pH 5, (Fig. 5b). This phenomenon was possibly linked to the strong electrostatic interaction that occurred between the positively charged ES-Zn complex and the negatively charged BSA molecules. Additionally, BSA molecules may form the metal chelate complex with ES-Zn adsorbent. The exposed electron-donating amino acid residues (e.g., imidazole group of histidine) on the surface of BSA may contribute to the binding of BSA molecules to Zn ions. Based on these experimental results, the subsequent adsorption studies were performed at pH 5 using ES-Zn adsorbents.

$$\text{ES-Zn}^{2+} + \text{BSA}^{x-} \Leftrightarrow \left(\text{ES-Zn}^{2+}\right)\text{-His-}(\text{BSA}^{x-})\text{(metal chelate complex)} \quad (8)$$

The adsorption of negatively charged BSA molecules onto ES-Zn adsorbents can be explained by the modified double-electric layer model proposed by Grahame (Grahame 1947). According to this model, the stern layer consists of two layers, namely the inner layer wherein the metal ions are attached to the negatively charged ES surface directly, and the outer layer wherein the adsorbed negative ions have a looser arrangement (Wang et al. 2015). The phenomena of BSA adsorption by ES-Zn adsorbents were similar to the adsorption behavior of dye as reported in a past study (Tsai et al. 2008) showing that the ES particles had a stronger affinity for the binding of negatively charged Orange 51 dye than that of the positively charged Blue 9. The similar results were observed in a previous study showing that the negatively charged arsenic, lignosulfonate, and phosphate ions can be highly adsorbed by ES particle (Zulfikar et al. 2012).

Influence of operating parameters on adsorption isotherm

The adsorption isotherms for the BSA binding onto ES-Zn complex at different working temperatures are illustrated in Fig. 6a–c. The adsorption data were fitted by three different isotherm models, including Langmuir, Freundlich, and Langmuir–Freundlich models.

The equilibrium adsorption data were satisfactorily correlated by the Langmuir–Freundlich model but not the Langmuir model and Freundlich model. The Langmuir–Freundlich model (Jeppu and Clement 2012) presumes that the adsorption of BSA molecules takes place on a heterogeneous surface. As the temperature increased from 277 to 323 K, the equilibrium association constant increased from 1.55×10^2 to 1.45×10^3 (mL solution/mg BSA), as shown in Fig. 6c. The maximum binding capacity of ES-Zn complexes was increased from 25.22 to 34.28 (mg BSA/g ES-Zn), as shown in Fig. 6a, b. The increase in binding capacity of ES-Zn along with the increase in temperature indicated that the binding of BSA is endothermic in nature (Ahmad et al. 2012). An increase in the binding capacity was believed to be caused by the intensification of the collision frequency between ES-Zn adsorbent and BSA. The values of the standard deviation for the best-fit model were less than 5%. The values of n decreased with the increasing temperature, indicating a decrease in binding cooperativity. Furthermore, based on Table 2, the values of correlation coefficient for Langmuir–Freundlich plots at 277–323 K were much higher than that for Langmuir and Freundlich models; hence, it is proposed that the equilibrium statistics are appropriately defined by Langmuir–Freundlich isotherm.

The equilibrium adsorption curves were steeper at a higher temperature, indicating a greater binding strength between BSA and ES-Zn complexes. This was due to the fact that the metal-chelate binding was the main force during the BSA adsorption process (Masuoka et al. 1993). However, retention of BSA molecule on the ES-Zn complexes may be a combined effect of electrostatic and/or metal-ion-chelating interactions. The Langmuir–Freundlich model can explain the sigmoidal shape of the experimental profile resulted primarily from the above-mentioned cooperative interaction.

Changes in the apparent thermodynamic parameters

As given in Table 3, in the range of 277–323 K, the negative values of ΔG° confirmed the spontaneous nature of the BSA adsorption by ES-Zn complexes. An increase in the temperature led to an increase in the absolute value of ΔG° which indicates a greater affinity of BSA to ES-Zn complexes at a higher temperature condition. The change in ΔG° ranged from -20 to 10 kJ/mol; hence, the removal of BSA is a physical binding process (Chabani et al. 2006). The positive value of ΔH° indicated that the adsorption of BSA was an endothermic reaction and was favorable at a higher temperature (Fig. 6). The positive value of ΔS° indicated that there is an upsurge in the randomness in the solid/liquid interface during the binding process (Gupta and Ali 2000).

Influence of operating parameters on kinetic of BSA adsorption

The kinetic of BSA adsorption was investigated to determine the time required to attain an equilibrium and to elucidate the mechanism of the adsorption. Adsorption of BSA on the porous adsorbents normally undergoes four phases: bulk diffusion, film diffusion, intra-particle diffusion, and lastly the attachment of BSA onto the binding sites (Graham and

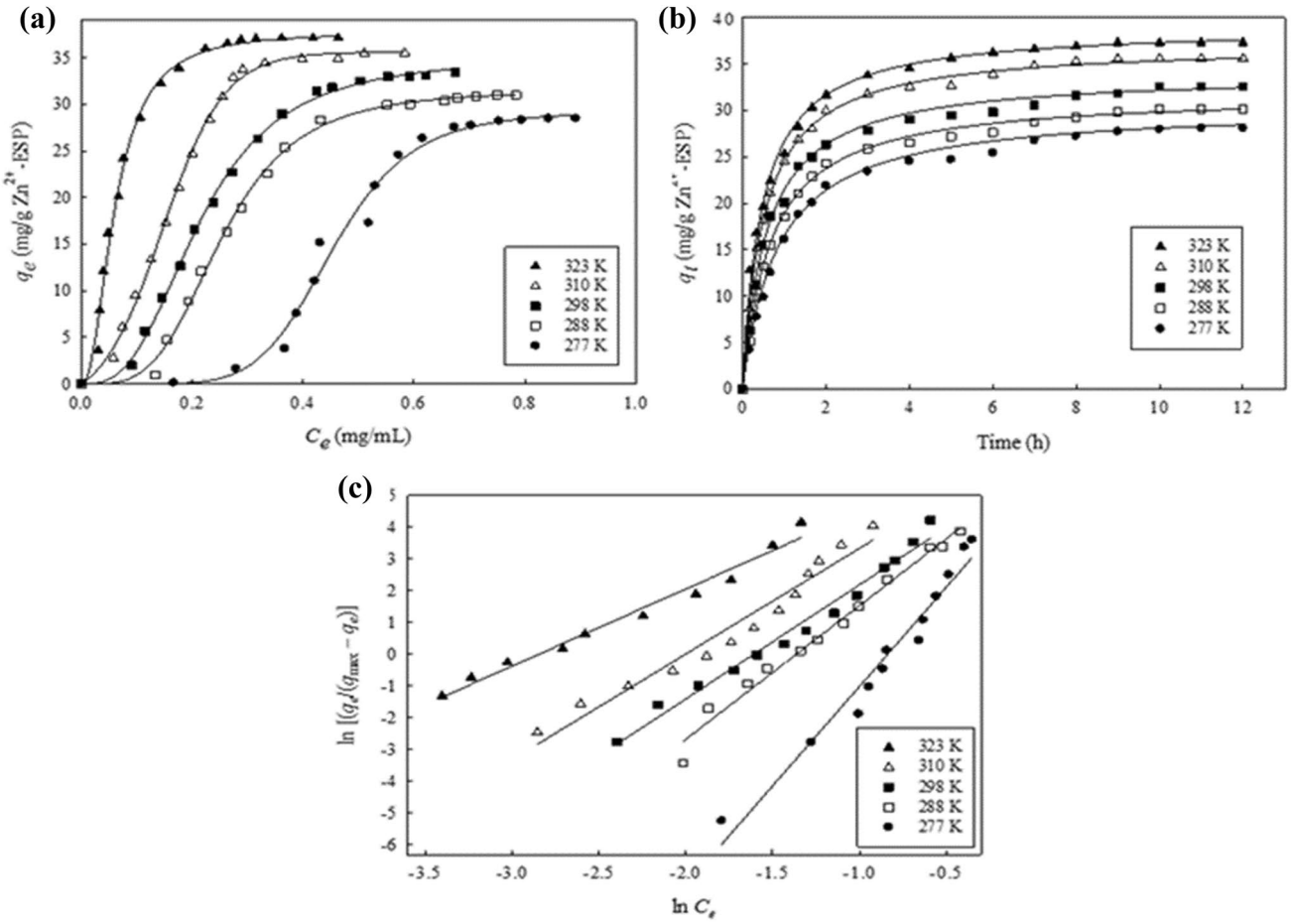

Fig. 6 **a** Adsorption isotherm of BSA by ES-Zn complexes at different temperatures. **b** Time course of BSA adsorption by ES-Zn complexes at different temperatures. **c** Langmuir–Freundlich isotherm plot for adsorption of BSA by ES-Zn complexes at different temperatures

Fook 1982). The kinetics of adsorption of BSA onto ES was studied by using three models, including pseudo-first-order, pseudo-second-order, and intra-particle diffusion models.

Table 2 Comparison of regression coefficients (R^2) for Langmuir, Freundlich, and Langmuir–Freundlich isotherms at different removal temperatures

Temperature (K)	Langmuir	Freundlich	Langmuir–Freundlich
323	0.7602	0.8555	0.9780
310	0.0472	0.8573	0.9601
298	0.0421	0.8862	0.9810
288	0.1045	0.8287	0.9840
277	0.3247	0.8728	0.9629

Kinetics of BSA adsorption by ES-Zn complexes

The rate of adsorption of BSA onto ES-Zn adsorbents was investigated at varying temperatures (277–323 K), and the results are presented in Fig. 7b, c. The results revealed that the initial adsorption rate increased following a rise in the temperature, and the adsorption rate reached a constant after approximately 6 h. The values of $q_{max,cal}$ increased from 30.4 to 38.9 (mg BSA/g ES-Zn) as the temperature increased from 277 to 310 K. Given that the rate of chemisorption increased with an increase in temperature, the mechanism of BSA adsorption was believed to involve the chemical interaction, for example metal-chelate binding. In this case, a rise in temperature caused a stronger binding force between BSA and ES-Zn complexes. Thus,

Table 3 Thermodynamic parameters calculated from Langmuir–Freundlich model for BSA adsorption by ES-Zn complexes at different operating temperatures

Temperature (K)	$q_{max\ (exp)}$ (mg/g)	n	K_d^* (mg/mL)	R^2	K_{ads} (mL/mg)	ΔG°_{ads} (kJ/mol)	ΔH°_{ads} (kJ/mol)	ΔS°_{ads} (J/mol K)
323	37.10	2.427	9.98×10^{-4}	0.9780	1002.0	−18.56	27.61	143.02
310	35.51	3.325	1.28×10^{-3}	0.9601	781.3	−17.17	–	–
298	33.47	3.594	3.07×10^{-3}	0.9810	325.7	−14.34	–	–
288	31.01	4.213	3.18×10^{-3}	0.9840	314.5	−13.77	–	–
277	28.49	6.262	5.23×10^{-3}	0.9629	191.2	−12.10	–	–

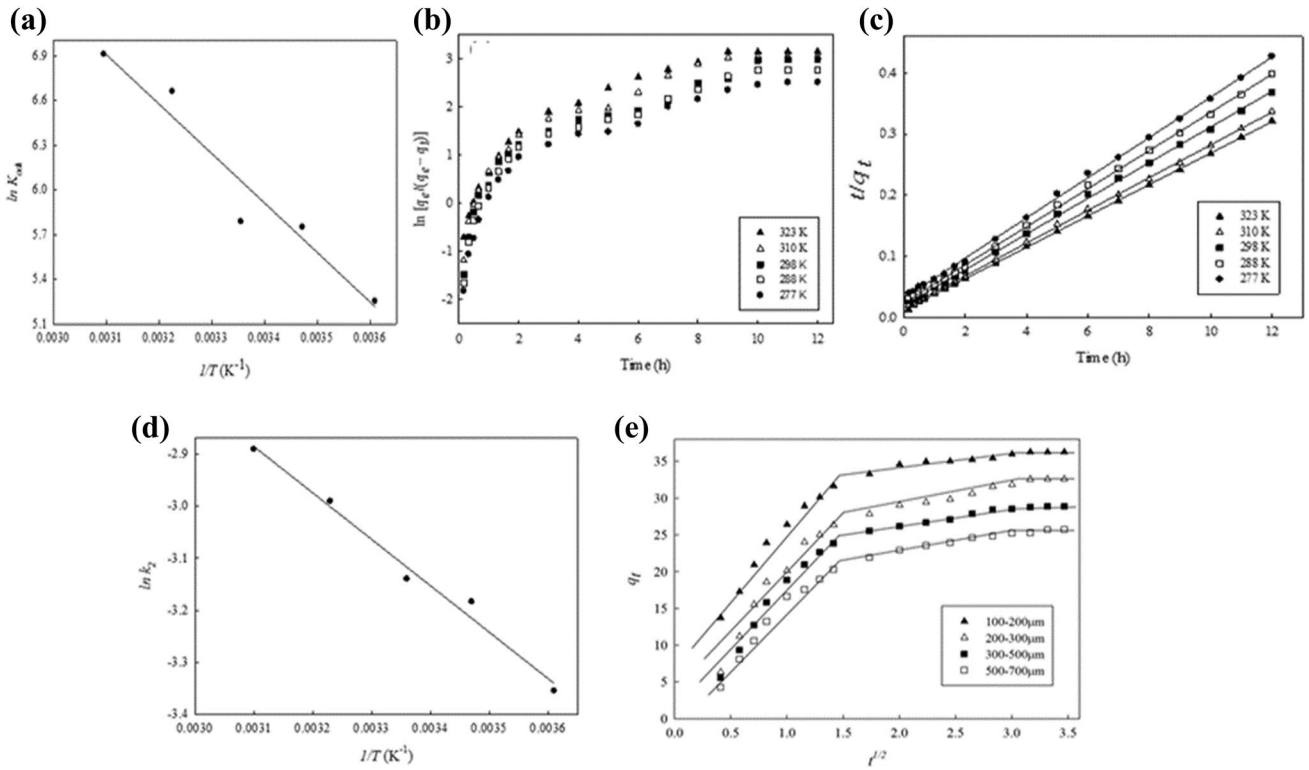

Fig. 7 **a** van't Hoff plots for the adsorption of BSA by ES-Zn complexes. Regressions of kinetic plots of BSA adsorption by ES-Zn complexes at different temperatures using **b** pseudo-first-order model and **c** pseudo-second-order model. **d** Arrhenius plot of ln k_2 against $1/T$ for the adsorption of BSA by Zn-ES complexes. **e** Intra-particle diffusion plot for BSA adsorption by different sizes of ES-Zn complexes

the adsorption capacity of ES-Zn complexes at high temperature was greater.

The correlation coefficients were found to be low in value for pseudo-first-order kinetic model (Table 4) and were not used to express the BSA adsorption process. As for the pseudo-second-order kinetic model, the correlation coefficients were found to be higher (0.999) at the operating temperature of 323 K. As shown in Fig. 7b, c, this was found to be considerably higher than other kinetic models assessed. Therefore, the pseudo-second-order kinetic model showed the best fit for the adsorption of BSA onto ES-Zn adsorbent. Based on the pseudo-second-order kinetic model, the rate constant is governed by temperature according to Arrhenius equation and is illustrated in Fig. 7d.

Based on the experimental data evaluated in the temperature range of 277–323 K, the activation energy for adsorption of BSA by ES-Zn complexes was 7.323 kJ/mol. Hence, the adsorption of BSA by ES-Zn complexes is an endothermic process. The rate constant, k_2, was found to increase from 3.49×10^{-2} to 5.55×10^{-2} mg BSA/min g ES-Zn along with the rise in temperature from 277 to 310 K. This was due to the increase in the kinetic energy of BSA molecules,

Table 4 Kinetic constants calculated from pseudo-first-order, pseudo-second-order, and intra-particle diffusion model for the adsorption of BSA by ES-Zn complexes

Temperature (K)	Pseudo-first-order kinetic model		Pseudo-second-order kinetic model					Intra-particle diffusion model			
	k_1 (1/h)	R^2	k_2 (g/mg h)	$q_{2(exp)}$ (mg/g)	$q_{2(cal)}$ (mg/g)	*Ea* (kJ/mol)	R^2	k_p (mg/g $h^{1/2}$)		R^2	
								First stage	Second stage	First stage	Second stage
323	0.295	0.8332	0.0555	37.30	38.91	7.323	0.9999	19.748	2.7999	0.9925	0.9739
310	0.296	0.8212	0.0502	35.61	37.31	(R^2 0.9834)	0.9998	19.996	3.2411	0.9569	0.9658
298	0.296	0.8235	0.0433	32.58	34.25	–	0.9994	19.434	2.8775	0.9554	0.9724
288	0.295	0.8067	0.0414	30.14	32.05	–	0.9995	19.778	3.2459	0.9807	0.9581
277	0.294	0.7972	0.0349	28.10	30.40	–	0.9993	17.788	2.6756	0.9911	0.9578

thereby increasing their mobility and improving their interaction with the adsorption sites at the surface of ES-Zn complexes. Several factors, including conformational structure of BSA, characteristics of ES, and the experimental conditions, are likely to affect the kinetic rate of BSA adsorption onto ES-Zn complex.

Intra-particle diffusion model

A sequential multi-step mechanism was involved in the adsorption of BSA onto ES-Zn complexes: (1) mass transfer of BSA from bulk phase to the surface of ES-Zn complexes, (2) removal at a site on the surface, and (3) intra-particle diffusion of the BSA molecules to a binding site by pore diffusion. As shown in Fig. 7e, the plots of q_t versus $t^{0.5}$ at different temperatures displayed a multi-linearity relation, indicating that BSA adsorption was affected by several processes. Furthermore, none of the plots intersected the origin, indicating that the intra-particle diffusion was not the only rate-controlling step. The adsorption rate can be regulated by other kinetic mechanisms as reported previously (Doğan et al. 2004; Tofighy and Mohammadi 2011).

The values of k_i and C (intercept) obtained from the linear regression analysis of each stage of BSA adsorption are listed in Table 5. It was proposed that BSA molecules diffused from the liquid phase to the mesopore region and then to the micropore region in the ES particles. The diffusion rate in the micropore region was lower than in mesopore region, indicating the multistage kinetic characteristic of diffusion. The micropore diffusion is considered as the rate-determining step for the whole process of pore diffusion. It has been confirmed that the pore size distribution in ES particles is multimodal, and the significant mean pore diameters are 1.0 nm, 1.3 nm, and 50 nm. Hence, the multistage adsorption processes were observed. The rate of adsorption may be controlled by the diffusion via micropores. Based on the results, it was observed that the adsorption rates are in the descending order of first stage ($k_{i,1}$) > second stage ($k_{i,2}$) > third stage ($k_{i,3}$). The changes in k_i values could be attributed to the adsorption of BSA on the external surface, mesopore region, transition pore region, and micropore region, respectively.

Regeneration and repeated use of ES particle

Imidazole and EDTA were chosen as the reagents for regenerating ES-Zn adsorbents for the repeated uses of adsorbents. The performance of ES-Zn regeneration was investigated by a series of step changes in the concentration of eluents (100–1000 mM, 10 mL in each step). Table 6 shows the concentration of BSA eluted over a wide range of imidazole concentration. The elution efficacy was dependent on the binding strength of Zn–BSA onto the ES particle. The

Table 5 Intra-particle kinetics rate constants calculated from intra-particle diffusion model for different stages of BSA adsorption by ES-Zn complexes

Particles size (μm)	First stage		Second stage		Third stage
	k_{p1} (mg/g $h^{1/2}$)	R^2	k_{p2} (mg/g $h^{1/2}$)	R^2	k_{p3} (mg/g $h^{1/2}$)
100–200	17.773	0.9709	1.5583	0.9122	–
200–300	19.434	0.9554	2.8775	0.9724	–
300–500	18.284	0.9729	2.1036	0.9601	–
500–700	15.712	0.9652	2.1671	0.9687	–

Table 6 Effect of concentration of imidazole and EDTA on the elution of BSA

Eluent (mM)	Eluted BSA (%)	
	Imidazole	EDTA
100	8.29	26.74
200	5.39	18.39
400	5.63	15.90
600	2.04	13.43
800	0.58	12.91
1000	–	12.78
Total (%)	21.93	100.12

overall yield of eluted BSA was only 21.93%, suggesting that the rest of adsorbed BSA (79%) occupied the binding sites of ES tightly. The secondary eluent, EDTA (100–1000 mM) was then used to elute the remaining adsorbed BSA. From the results, the adsorbed BSA was eluted in various proportions and could be completely eluted by 1000 mM of EDTA. The subsequent experiments have confirmed that the adsorbed Zn–BSA chelates on the ES particle can be fully eluted with 10 mL of 1000 mM EDTA in a single step. In other words, ES particles can be regenerated by using EDTA. The amounts of heavy metal and soluble protein adsorbed by the regenerated ES particle were not affected by the repeated uses of ES particle.

Remarks on mechanisms of removal of metal ions and soluble proteins by ES

The kinetic adsorption behavior of ES on metal ion and soluble was affected by the shape and size of the container. The rate of BSA adsorption under the optimized operating conditions was not significantly affected by 20 rpm of rotational speed and 45° of rotational disk angle. It was observed that a lower or higher rotational speed of the rotator may cause aggregation, overlapping, or overcrowding of ES particles. This resulted in decrease in the available surface area and binding capacity of ES. Hence, the 15-mL centrifuge tube was chosen in the experiments. However, considering the scale-up process, the selection of a suitable container and rotator is crucial for improving the kinetic rate of BSA adsorption.

With respect to ES particles, the principles of ion exchange and/or electrostatic interaction are the most probable adsorption mechanism(s) for the removal of heavy metal from wastewater. However, as the pH for adsorption is high (pH > 10), micro-precipitation on the ES surface may occur. The adsorption of protein on ES-M complexes was believed to be governed by mechanisms such as coordination and metal chelation. All the adsorption mechanisms as indicated above may work together to govern the adsorption of soluble protein on ES-M complexes. Based on the results of BSA desorption by EDTA, the interaction between metal and protein may be based on metal chelation, rather than the ionic interaction.

In a study conducted by Dizge and Tansel (2011), the model SMPs made of carbohydrates (represented by glucose) and protein (represented by BSA) were treated by activated carbon, and the maximum adsorption capacity of activated carbon for BSA was 9.7 mg/g. This reported adsorption capacity of activated carbon was much lower than that of our ES-Zn complexes, which recorded a 3.45-fold increment in BSA adsorption (corresponding to 33.47 mg/g). The regeneration of exhausted activated carbon by chemical and thermal procedures is also expensive and can result in the loss of adsorbent (Jiuhui 2008). Therefore, the use of discarded ES waste as a treatment for heavy metals and soluble proteins from wastewater is a very feasible method.

Conclusions

The potential application of ES waste as an economical biological adsorbent for the removal of heavy metal ions and BSA (as a model protein of SMP) was presented in this study. The adsorption of BSA on ES-Zn complex was best described by the pseudo-second-order kinetic model. The decoration of heavy metal ion on the ES renders an effective pseudo-chelating property to the ES-M adsorbents for the removal of BSA. The adsorbed Zn–BSA chelates were found to be stable on ES particle, indicating the minimal secondary pollution caused by the release of metallic Zn ions. This approach offers an attractive avenue to the removal of both Zn and SMP, which are the main pollutants in the aquatic environment. This study reveals a novel technique for heavy

metal removal using waste ES which is considered as a bioremediation approach in treating contaminated water. This strategy can also be adopted as a pretreatment step for membrane filtration used in the treatment of wastewater. The successful removal of Zn–BSA complex from the ES particles allows the regeneration of adsorbent for reuse purposes.

Acknowledgements YKC gratefully acknowledges the financial support provided by the Ministry of Science and Technology of Taiwan (Grant Numbers: MOST 104-2622-E-131-021 and MOST 103-2622-E-131-CC3).

References

Abollino O, Aceto M, Malandrino M, Sarzanini C, Mentasti E (2003) Adsorption of heavy metals on Na-montmorillonite. Effect of pH and organic substances. Water Res 37(7):1619–1627. https://doi.org/10.1016/S0043-1354(02)00524-9

Ahmad R, Kumar R, Haseeb S (2012) Adsorption of Cu^{2+} from aqueous solution onto iron oxide coated eggshell powder: evaluation of equilibrium, isotherms, kinetics, and regeneration capacity. Arab J Chem 5:353–359. https://doi.org/10.1016/j.arabjc.2010.09.003

Ahmed IT, Ahmed Boraei AA, El-Roudi OM (1998) Mixed-ligand complexes of some divalent transition metal ions with dicarboxylic amino acids and 8-hydroxyquinoline. J Chem Eng Data 43:459–464. https://doi.org/10.1021/je970192m

Al-Ghouti MA, Salih NR (2018) Application of eggshell wastes for boron remediation from water. J Mol Liq 256:599–610. https://doi.org/10.1016/j.molliq.2018.02.074

Atia KS, El-Arnaouty MB, Ismail SA, Dessouki AM (2003) Characterization and application of immobilized lipase enzyme on different radiation grafted polymeric films: assessment of the immobilization process using spectroscopic analysis. J Appl Polym Sci. https://doi.org/10.1002/app.12620

Babel S, Kurniawan TA (2003) Low cost adsorbents for heavy metals uptake from contaminated water: a review. J Hazard Mater B97:219–243. https://doi.org/10.1016/S0304-3894(02)00263-7

Barker Duncan J, Stuckey DC (1999) A review of soluble microbial products (SMP) in wastewater treatment systems. Water Res 33:3063–3082

Chabani M, Amrane A, Bensmaili A (2006) Kinetic modelling of the adsorption of nitrates by ion exchange resin. Chem Eng J 125:111–117. https://doi.org/10.1016/j.cej.2006.08.014

De Angelis G, Medeghini L, Conte AM, Mignardi S (2017) Recycling of eggshell waste into low-cost adsorbent for Ni removal from wastewater. J Clean Prod 164:1497–1506. https://doi.org/10.1016/j.jclepro.2017.07.085

Di Russo NV, Estrin DA, Martí MA, Roitberg AE (2012) pH-dependent conformational changes in proteins and their effect on experimental pKas: the case of nitrophorin 4. PLoS Comput Biol 8:e1002761. https://doi.org/10.1371/journal.pcbi.1002761

Dizge N, Tansel B (2011) Multiparametric investigation of competitive and noncompetitive sorption characteristics of SMP fractions (carbohydrate and protein) on activated carbon. J Hazard Mater 185(2–3):996–1004. https://doi.org/10.1016/j.jhazmat.2010.10.004

Doğan M, Alkan M, Türkyilmaz A, Özdemir Y (2004) Kinetics and mechanism of removal of methylene blue by adsorption onto perlite. J Hazard Mater 109:141–148. https://doi.org/10.1016/j.jhazmat.2004.03.003

Dunbar RC, Steill JD, Polfer NC, Oomens J (2009) Dimeric complexes of tryptophan with M^{2+} metal ions. J Phys Chem A 113:845–851. https://doi.org/10.1021/jp8087176

Graham EE, Fook CF (1982) Rate of protein absorption and desorption on cellulosic ion exchangers. AIChE J 28:245–250. https://doi.org/10.1002/aic.690280212

Grahame DC (1947) The electrical double layer and the theory of electrocapillarity. Chem Rev 41:441–501. https://doi.org/10.1021/cr60130a002

Gupta VK, Ali I (2000) Utilisation of bagasse fly ash (a sugar industry waste) for the removal of copper and zinc from wastewater. Sep Purif Technol 18:131–140. https://doi.org/10.1016/S1383-5866(99)00058-1

Jarusutthirak C, Amy G (2006) Role of soluble microbial products (SMP) in membrane fouling and flux decline. Environ Sci Technol 40:969–974. https://doi.org/10.1021/es050987a

Jeppu GP, Clement TP (2012) A modified Langmuir–Freundlich isotherm model for simulating pH-dependent adsorption effects. J Contam Hydrol 129–130:46–53. https://doi.org/10.1016/j.jconhyd.2011.12.001

Jiuhui QU (2008) Research progress of novel adsorption processes in water purification: a review. J Environ Sci 20(1):1–13. https://doi.org/10.1016/S1001-0742(08)60001-7

Kunacheva C, Stuckey DC (2014) Analytical methods for soluble microbial products (SMP) and extracellular polymers (ECP) in wastewater treatment systems: a review. Water Res 61:1–18. https://doi.org/10.1016/j.watres.2014.04.044

Loukidou MX, Matis KA, Zouboulis AI, Liakopoulou-Kyriakidou M (2003) Removal of As(V) from wastewaters by chemically modified fungal biomass. Water Res 37(18):4544–4552. https://doi.org/10.1016/S0043-1354(03)00415-9

Masuoka J, Hegenauer J, Van Dyke BR, Saltman P (1993) Intrinsic stoichiometric equilibrium constants for the binding of zinc(II) and copper(II) to the high affinity site of serum albumin. J Biol Chem 268:21533–21537

Matilainen A, Vepsäläinen M, Sillanpää M (2010) Natural organic matter removal by coagulation during drinking water treatment: a review. Adv Colloid Interface Sci 159:189–197. https://doi.org/10.1016/j.cis.2010.06.007

Mopoung S, Jitchaijaroenkul K (2017) Characterization of activated carbon from eggshell membranes prepared using sodium acetate and zinc metal activation. Am J Appl Sci 14:737–747. https://doi.org/10.3844/ajassp.2017.737.747

Mosaddegh E, Hassankhani A (2014) Preparation and characterization of nano-CaO based on eggshell waste: novel and green catalytic approach to highly efficient synthesis of pyrano[4,3-b] pyrans. Chin J Catal 35:351–356. https://doi.org/10.1016/S1872-2067(12)60755-4

Oliveira LC, Petkowicz DI, Smaniotto A, Pergher SB (2004) Magnetic zeolites: a new adsorbent for removal of metallic contaminants from water. Water Res 38(17):3699–3704. https://doi.org/10.1016/j.watres.2004.06.008

Pachapur VL, Das RK, Brar SK et al (2017) Valorization of crude glycerol and eggshell biowaste as media components for hydrogen production: a scale-up study using co-culture system. Bioresour Technol 225:386–394. https://doi.org/10.1016/j.biortech.2016.11.114

Podstawczyk D, Witek-Krowiak A, Chojnacka K, Sadowski Z (2014) Biosorption of malachite green by eggshells: mechanism identification and process optimization. Bioresour Technol 160:161–165. https://doi.org/10.1016/j.biortech.2014.01.015

Pramanpol N, Nitayapat N (2006) Adsorption of reactive dye by eggshell and its membrane. Kasetsart J Nat Sci 40:192–197

Robinson T, Chandran B, Nigam P (2002) Removal of dyes from an artificial textile dye effluent by two agricultural waste residues,

corncob and barley husk. Environ Int 28(1–2):29–33. https://doi.org/10.1016/S0160-4120(01)00131-3
Shaheen SM, Eissa FI, Ghanem KM et al (2013) Heavy metals removal from aqueous solutions and wastewaters by using various byproducts. J Environ Manag 128:514–521. https://doi.org/10.1016/j.jenvman.2013.05.061
Shi Q, Zhou Y, Sun Y (2008) Influence of pH and ionic strength on the steric mass-action model parameters around the isoelectric point of protein. Biotechnol Prog 21:516–523. https://doi.org/10.1021/bp049735o
Smith SC, Ahmed F, Gutierrez KM, Frigi Rodrigues D (2014) A comparative study of lysozyme adsorption with graphene, graphene oxide, and single-walled carbon nanotubes: potential environmental applications. Chem Eng J 240:147–154. https://doi.org/10.1016/j.cej.2013.11.030
Stadelman W (2000) Eggs and egg products. In: Francis FJ (ed) Encyclopedia of food science and technology, 2nd edn. Wiley, Hoboken, pp 593–599
Tofighy MA, Mohammadi T (2011) Adsorption of divalent heavy metal ions from water using carbon nanotube sheets. J Hazard Mater 185:140–147. https://doi.org/10.1016/j.jhazmat.2010.09.008
Tran VS, Ngo HH, Guo W et al (2015) Typical low cost biosorbents for adsorptive removal of specific organic pollutants from water. Bioresour Technol 182:353–363. https://doi.org/10.1016/j.biortech.2015.02.003
Trzaskowski B, Adamowicz L, Deymier PA (2007) A theoretical study of zinc(II) interactions with amino acid models and peptide fragments. J Biol Inorg Chem 13:133–137. https://doi.org/10.1007/s00775-007-0306-y
Tsai WT, Yang JM, Lai CW et al (2006) Characterization and adsorption properties of eggshells and eggshell membrane. Bioresour Technol 97:488–493. https://doi.org/10.1016/j.biortech.2005.02.050
Tsai WT, Hsien KJ, Hsu HC et al (2008) Utilization of ground eggshell waste as an adsorbent for the removal of dyes from aqueous solution. Bioresour Technol 99:1623–1629. https://doi.org/10.1016/j.biortech.2007.04.010
Wang X, Herting G, Odnevall Wallinder I, Blomberg E (2015) Adsorption of bovine serum albumin on silver surfaces enhances the release of silver at pH neutral conditions. Phys Chem Chem Phys 17:18524–18534. https://doi.org/10.1039/C5CP02306H
Wu J (2014) Eggs and egg products processing. In: Clark S, Jung S, Lamsal B (eds) Food processing. Wiley, Chichester, pp 437–455
Zaman T, Mostari MS, Al Mahmood MA et al (2018) Evolution and characterization of eggshell as a potential candidate of raw material. Cerâmica 64:236–241. https://doi.org/10.1590/0366-69132018643702349
Zhang Y, Chen Y, Westerhoff P, Hristovski K, Crittenden JC (2008) Stability of commercial metal oxide nanoparticles in water. Water Res 42(8–9):2204–2212. https://doi.org/10.1016/j.watres.2007.11.036
Zulfikar MA, Mariske ED, Djajanti SD (2012) Adsorption of lignosulfonate compounds using powdered eggshell. Songklanakarin J Sci Technol 34:309–316

Affiliations

Revathy Sankaran[1] · Pau Loke Show[2] · Chien-Wei Ooi[3] · Tau Chuan Ling[1] · Chen Shu-Jen[4] · Siao-Ying Chen[5] · Yu-Kaung Chang[5]

[1] Institute of Biological Sciences, Faculty of Science, University of Malaya, 50603 Kuala Lumpur, Malaysia

[2] Department of Chemical Engineering and Environmental Engineering, University of Nottingham Malaysia Campus, Semenyih, Selangor Darul Ehsan, Malaysia

[3] Chemical Engineering Discipline, School of Engineering, Monash University Malaysia, Jalan Lagoon Selatan, 47500 Bandar Sunway, Selangor, Malaysia

[4] Department of Chemical Engineering and Materials Engineering, National Kaohsiung University of Science and Technology, Kaohsiung City 80778, Taiwan

[5] Department of Chemical Engineering, Graduate School of Biochemical Engineering, Ming Chi University of Technology, New Taipei City 24301, Taiwan